Analyst

ROYAL SOCIETY OF CHEMISTRY

PAPER

View Article Online
View Journal | View Issue

Cite this: *Analyst*, 2025, **150**, 1303

Raman spectroscopy of ovarian and peritoneal tissue in the assessment of ovarian cancer†

Diana Frimpong, [a] Angela C. Shore,[a] Benjamin Gardner, [c] Claire Newton,[b] Joya Pawade,[d] Jonathan Frost, [e] Laura Atherton[e] and Nick Stone *[c]

Received 4th October 2024,
Accepted 27th February 2025

DOI: 10.1039/d4an01293c

rsc.li/analyst

During post chemotherapy surgery for ovarian cancer, it is important to ensure that any residual disease is carefully assessed and removed. The assessment remains subjective, despite clear evidence of the benefits of complete macroscopic resection. In this work, we have considered Raman spectroscopy as a possible tool for residual disease assessment by exploring its ability to correctly classify ovarian cancer from benign and borderline tissues. Samples from seventy-three participants were analysed (n = 20 benign, n = 11 borderline and n = 42 cancer) using a multivariate analysis model. All models shown utilised validation with leave one participant out cross-validation. In ovarian tissue this model achieved 94% sensitivity and 98% specificity for prediction of cancer from benign and 98% sensitivity and 89% specificity for prediction of cancer from borderline. Thorough assessment of the surrounding peritoneal tissues is extremely important. For these peritoneal tissues taken from participants with advanced ovarian cancer, the model achieved 78% sensitivity and 84% specificity for prediction of cancerous peritoneum from benign peritoneum in participants who had primary surgery and 68% sensitivity and 81% specificity in participants who had post chemotherapy surgery. This demonstrates viability of Raman spectroscopy for assessment of ovarian cancer.

Introduction

Ovarian cancer is the leading cause of death in gynaecological cancers[1] and accounts for 2% of all new cancers.[2] The prognosis, more so in advanced disease, remains poor with a five-year survival of 32% and 16% if diagnosed at stage III and stage IV disease respectively.[3]

Current evidence is clear on the survival benefits of achieving complete macroscopic resection or as a minimum, less than 1 cm residual disease,[4] however, this remains a subjective assessment, as no objective tool for residual disease volume assessment exists. Delaying surgery for primary chemotherapy has been demonstrated to be better for post operative outcomes,[5] and non-inferior to primary surgery for progression free survival.[5,6] However, achieving complete resection at interval debulking surgery (IDS) can be complicated by the fibrotic changes that occur as a result of primary chemotherapy.[6]

There is a need for a non-destructive tool that can accurately differentiate normal and fibrotic tissue from cancer, that is amenable to intraoperative use and can relay results in real time. One tool that has been explored for its biological applications is Raman spectroscopy.[7] This is a technique that uses the inelastic scattering of light to determine the molecular composition of a sample.[8] This technique has great potential for biomedical use. It has been demonstrated to be accurate for tumour excision margin assessment[9] and lymph node assessment[10] in breast cancer surgery and meets the aforementioned criteria for intraoperative assessment in ovarian cancer treatment.

There is previous work exploring the use of Raman spectroscopy to classify ovarian cancer however the body of work is limited when compared to other tumour sites and in exploring ovarian and peritoneal tissue in this context. The peritoneum is a common site of spread for ovarian cancer[11] and presence of peritoneal disease suggests advanced stage ovarian cancer (stage III or IV).[12] It would be futile to explore novel diagnostics for advanced ovarian cancer without including tissue from peritoneal disease. In 2007, Krishna *et al.* examined the biological differences of malignant ovarian tissue compared to normal and benign tissues using Raman spectroscopy. They concluded that lipids and DNA vibrations were the main differ-

[a]*NIHR Exeter Clinical Research Facility and Clinical and Biomedical Sciences, Faculty of Health and Life Sciences, University of Exeter, Exeter, Devon, UK*
[b]*University Hospitals Bristol and Weston NHS Trust, Bristol, UK*
[c]*Physics and Astronomy, Faculty of Environment, Science and Economy, University of Exeter, Exeter, Devon, UK. E-mail: n.stone@exeter.ac.uk*
[d]*Severn Pathology Services, North Bristol NHS Trust, Bristol, UK*
[e]*Royal United Hospitals Bath NHS Foundation Trust, Bath, UK*

† Electronic supplementary information (ESI) available. See DOI: https://doi.org/10.1039/d4an01293c

entiating features.[13] This finding was supported by the work by Maheedhar *et al*. in 2008 where they identified amide I and III from proteins, lipids, shift in δCH_2 and DNA as the features with relatively higher expression that distinguish cancer from normal. They also achieved a sensitivity of 88% and specificity of 84% for classifying cancer using principal component analysis-based model (PCA), with only eight participants without cancer and seven with ovarian cancer. Independent testing of this model with a limited number of participants achieved a sensitivity and specificity of 100%.[14] Similar accuracy results using leave one patient out cross validation (sensitivity 93% and specificity of 88%) were achieved by David *et al*. for cancer detection using ovarian and endometrial cancer tissue samples further highlighting the efficacy of the technique.[15]

Mice modelling of this concept of residual disease targeting using Raman spectroscopy was completed by Andreou *et al*. in 2019 where peritoneal cavities of mice with ovarian cancer were scanned using probes after local administration of nanoparticles.[16] This work highlights the feasibility of targeting metastases with vibrational spectroscopy techniques, however, although nanoparticles were locally applied, the currently unknown risks around retention of gold nanoparticles in this patient group is not ideal. Techniques to optimise Raman spectroscopy measuring only the native molecular signals, to achieve a similar aim are currently more likely to be adopted.

In this study, we aimed to assess Raman spectroscopy against histology for cancer detection in peritoneal and ovarian tissue and the effect of primary chemotherapy on detection accuracy. As such we have used tissue from women referred with suspected ovarian cancer, the outcome of which was either benign ovarian pathology, borderline ovarian tumour or ovarian cancer, of varying grades and stages of extent of disease. The importance of accurately discriminating cancer from these two ovarian pathology groups is highlighted by the Prostate, Lung, Colorectal and Ovarian cancer trial which demonstrated harm to women having extensive procedures to investigate suspected cancer.[17]

Table 1 Demographic information of participants in this study grouped by pathology class

Demographic information			
	Benign $n = 20$	Borderline $n = 11$	Cancer $n = 42$
Age (years)			
Mean (range)	57 (36–81)	55 (32–81)	62 (37–88)
No. of comorbidities			
0–2	8	4	21
3–5	9	5	19
6–8	3	2	2
Menopausal status			
Pre	4	3	2
Peri	0	2	1
Post	16	6	39
Smoking status			
Never smoked	13	7	23
Ex smoker	6	2	15
Smoker	1	2	4
Diagnosis			
	Fibroma	Serous tumour	High grade serous
	Dermoid	Mucinous tumour	Low grade serous
	Strum ovarii	Torsion/ necrosis	Clear cell
	Endometriosis		Mucinous
	Benign with small vessel vasculitis		Endometroid
	Mucinous cystadenoma		Granulosa cell tumour
	Serous cystadenoma		
Samples			
Ovarian	18	8	13 (2 NACT)
Peritoneal	9	1	24 (19 NACT)

NACT = Neoadjuvant chemotherapy.

Materials and methods

Live subject statement

This work was performed in accordance with NHS Health Research Authority (HRA) guidelines and approved by the North West – Preston Research Ethics Committee (REC). Following ethical approval, (IRAS ID 288711 – Molecular Spectroscopy in Identification and Assessment of Ovarian Cancer) eligible patients with suspected or confirmed ovarian cancer were recruited to the study. Written consent was obtained from participants in this study.

Tissue samples

Samples collected from 73 patients undergoing surgical treatment for suspected or confirmed ovarian cancer were included in this analysis. Table 1 details the demographic information of the participants in this study. Small (1 cm) areas of normal, suspicious (surgeon unsure if normal or cancer) and obvious cancer were removed, snap frozen in liquid nitrogen and then stored at −80 °C. For participants that had already received chemotherapy, a sample of representative fibrosis was also biopsied. No more than 4 samples were collected per participant.

As both ovarian and peritoneal samples were collected from two thirds of participants, there were 52 ovarian samples and 63 peritoneal samples. Samples were excluded due to damage, being too small to measure after sectioning and morphology being obscured by blood. Where there was a duplicate of the same tissue type and pathology from one participant, one slide as excluded. The remaining 39 ovarian samples and 34 peritoneal samples were used for this analysis.

Histological examination

Tissue samples were cryosectioned: three consecutive 20 μm sections were obtained. Section one and three were placed on a glass slide and underwent a manual staining process with haematoxylin and eosin (H&E). Section two was placed on a stainless steel slide and returned to the freezer for batch

ex vivo Raman spectroscopy measurements. All H&E slides were examined by a consultant pathologist to determine the status of the examined tissue, *i.e.* benign, borderline and cancer, as well as marking on the slides, areas with borderline tumour and cancer to be later correlated with the Raman tissue section.

Raman instrumentation and measurement protocol

Raman measurements were taken using a commercially available Raman spectrometer, Renishaw InVia Raman spectrometer. This was coupled with an 830 nm laser using a dichroic edge filter set and a Leica microscope. A grating of 600 lines per mm was used, and the system was calibrated using a Neon Argon lamp source and silicon and PTFE to check wavenumber position and basic alignment at the start of each set of measurements.

Tissue samples were defrosted at room temperature for a minimum of 10 minutes and then scanned using the white light image function of the InVia WiRE software. The area of interest previously marked on the H&E slide by a consultant histopathologist was matched to the Raman slide and a square grid of 300 μm by 300 μm was drawn over the area. Point measurements at 50 μm intervals were taken of the area covered by the grid, resulting in 49 spectra per area of interest. Each measurement was acquired for five seconds, with three accumulations using 100 mW laser power. RensihawWiRE software automated cosmic ray removal was enabled.

Data analysis

Pre-processing. Data analysis was carried out using MATLAB R2020b software. Saturated spectra were replaced with those located adjacent in the map, either the mean of the two spectra before and after, or two spectra before or two spectra after. The data was baselined using an in house script to remove background signal using asymmetric least squares fit and then vector normalised.

Analysis. The spectra were divided into their associated pathology groups and associated differences evaluated.

Multivariate analysis techniques were then used to explore models based on the data for the prediction of pathology. Principal component analysis (PCA), a technique used to the reduce data dimensions, was used to identify the variables (principal components) that explain the variance in the data. For each principal component (PC), the loadings represent the weight of the original spectral variables, and the scores explain the contribution of each PC to the individual spectrum.[18] Analysis of variance (ANOVA) was used to determine the statistically significant PCs. The scores of the PCs with statistical significance were used in combination with the pathology data to create a linear discriminant model for the separation of the data into groups. The classification performance of the model was then calculated. Leave-one-out (participant) cross validation, *i.e.* all samples and spectra from each individual in turn were removed from the dataset used to create the classification model and then they were used to evaluate the performance of the model for predicting the pathology of those samples. Sensitivity, specificity, accuracy, area under the curve and F1 score were calculated for the prediction performance. The F1 score is a blend of the precision and recall of the model and as such, takes into account how the data is distributed and penalizes models with a high false negative rate.[19]

Tentative peak assignments have been made using reference tables.[20–22]

Results

Ovarian tissue

1813 spectra (from 37 participants) were used for this analysis. The mean spectra of the pathology groups, benign, borderline and cancer, are displayed in Fig. 1.

Separation within the groups to varying levels is apparent even in this simple plot of group means. It is evident in the group comparisons in Fig. 1 that there is some overlap of variance within the pathology groups however there is still separation seen, such as in the cancer *versus* benign group at 1332 cm^{-1} suggesting increased nucleotides in the cancer group compared to the benign group. This is supported by the difference between the mean plot Fig. 2(d), which highlights the peaks suggesting an increase in concentration of lipids (545, 1074, 1119 & 1438 cm^{-1}), amino acids (642, 1001 & 1205 cm^{-1}), nucleotides (663, 711, 724, 777, 1256, 1332 & 1573 cm^{-1}) and amide I group (1652 cm^{-1}) in cancer. Peaks with a negative intensity value suggest lower concentration in cancer of phosphate minerals (591 cm^{-1}), collagen (812, 856, 919 & 935 cm^{-1}), amino acids (1035 & 1176 cm^{-1}), carotenoids (1159 cm^{-1}), amide III groups (1240 & 1276 cm^{-1}), CH_3 modes in proteins (1400 & 1415 cm^{-1}) and deoxyribose (1465 cm^{-1}) when compared to the benign group.

The cancer and borderline groups, Fig. 2(b) & (e), show their greatest differences with increased intensity in phosphates (1069 & 1095 cm^{-1}), collagen (892 cm^{-1}), ribose (912 cm^{-1}), amino acids (1000, 1360 & 1597 cm^{-1}), lipids (1118, 1442 cm^{-1}), cytosine (1255 cm^{-1}), nucleic acids (1327 & 1573 cm^{-1}), CH_3 bending mode (1386 cm^{-1}) and amide I

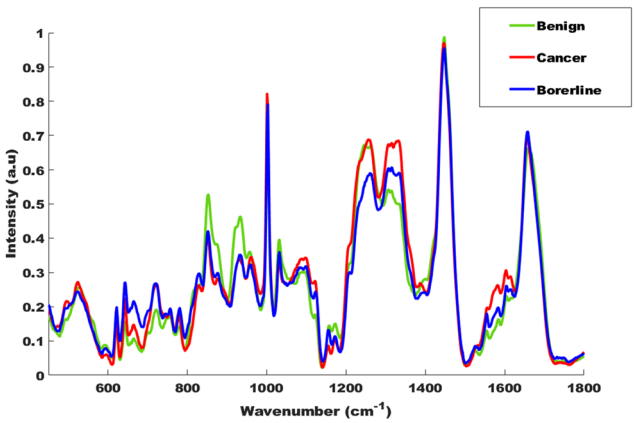

Fig. 1 Mean spectra of ovarian tissue for pathology groups benign (green), borderline (blue) and cancer (red).

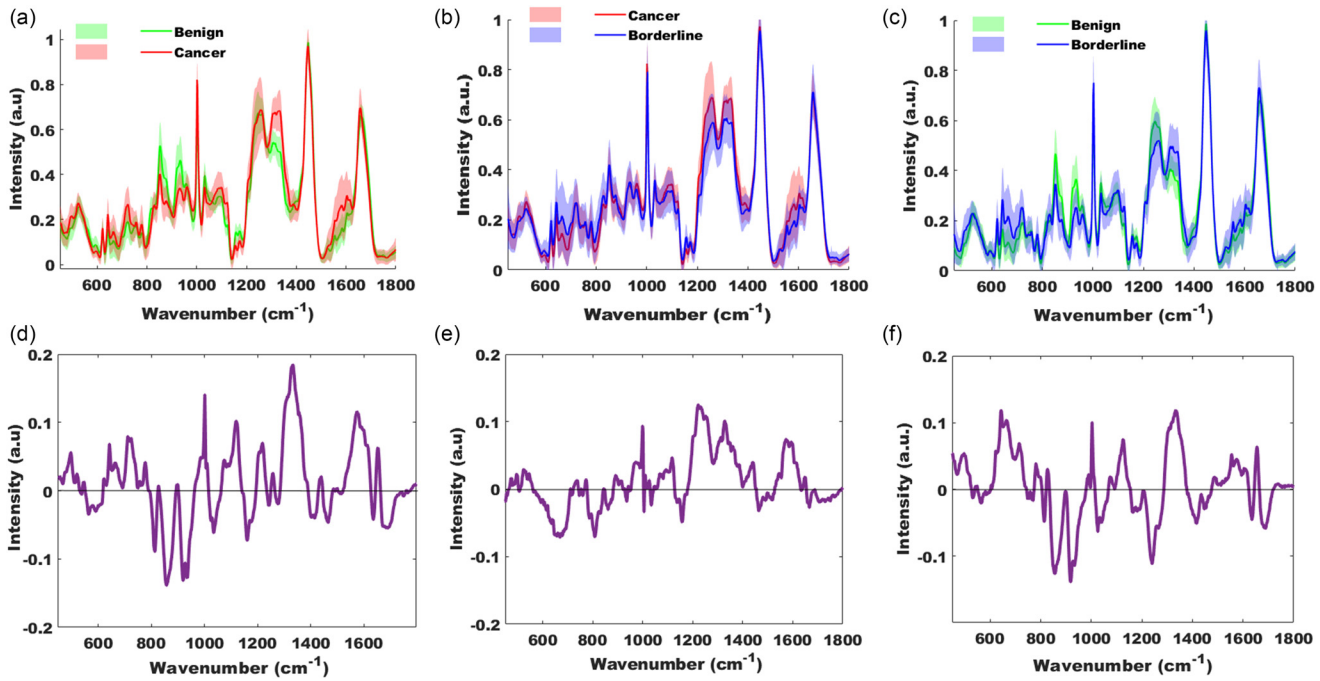

Fig. 2 Mean and standard deviation spectra of comparison of pathology groups for ovarian tissue. (a) Cancer *versus* benign (1421 spectra); (b) cancer *versus* borderline (931 spectra); (c) borderline *versus* benign (1274 spectra); (d), (e) and (f) are difference between spectra of the pathology groups from (a), (b) and (c) respectively.

(1650 cm^{-1}) in the cancer group and lower concentrations of thymine and guanine (broad peak 647–690 cm^{-1}), DNA (807 & 831 cm^{-1}), amino acids (1005, 1034 & 1176 cm^{-1}), collagen (861 & 936 cm^{-1}), carotenoids (1519 & 1158 cm^{-1}), deoxyribose (1464 cm^{-1}) and amide I group (1667 cm^{-1}) when compared to the borderline group.

The comparison of the two non-cancer groups, Fig. 2(c) & (f), suggests a higher concentration of amino acids (643, 1003 & 1555 cm^{-1}), nucleotides (666, 716, 981, 1336 & 1576 cm^{-1}), DNA (827 cm^{-1}), lipids (1074 & 1127 cm^{-1}) and amide I (1655 cm^{-1}) in the borderline group and lower concentrations of disulphide stretch in proteins (532 cm^{-1}), collagen (814, 855, 918 & 935 cm^{-1}), amino acids (1026 & 1040 cm^{-1}), amide III group (1242 cm^{-1}), CH_3 deformation (1415 cm^{-1}) and amide I group (1635 & 1690 cm^{-1}) compared to benign group.

PCA-LDA models using the significant PCs on ANOVA testing (p = 0.001) were used to classify the spectra into their groups *e.g.* benign, cancer *etc*. The model was able to classify cancer from benign and cancer spectra with a sensitivity of 98% and specificity of 100%. Leave one participant out cross validation of 882 benign and 539 cancer spectra achieved a sensitivity of 94% and specificity of 98%. The F1 score for this validation model was 0.95 and mean area under the curve following two-fold cross validation of 0.97 (Fig. 3). Exploring the principal component loadings as seen in the ESI (Fig. S1†) it is clear the key molecular differences are very similar to those identified from the difference spectra in Fig. 2(d) as discussed above.

Classification of cancer from borderline and cancer spectra achieved a sensitivity and specificity of 99%. Leave one participant out cross validation of 392 borderline and 539 cancer spectra achieved a sensitivity of 98% and specificity of 89%. The F1 score for this validation model was 0.94 and mean area under the curve following two-fold cross validation of 0.99.

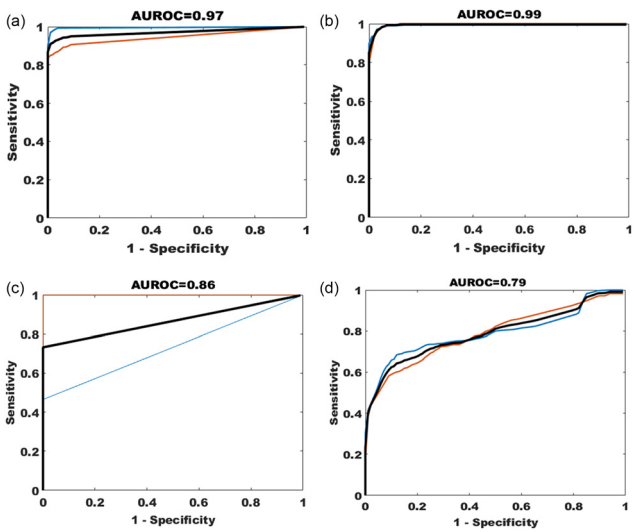

Fig. 3 Mean receiver operating curve following two-fold cross validation. The orange and blue lines show each iteration, and the black line shows the mean, with the area under the mean curve documented above the plot. (a) Ovarian tissue cancer *versus* benign; (b) Ovarian tissue cancer *versus* borderline; (c) Peritoneal tissue cancer *versus* benign; (d) Peritoneal tissue post chemotherapy (IDS) cancer *versus* benign.

Classification of borderline from benign and borderline spectra achieved a sensitivity of 90% and specificity of 95%. Leave one participant out cross validation of 882 benign and 392 borderline spectra achieved a sensitivity of 72% and specificity of 93%. The F1 score for this validation model was 0.77 and mean area under the curve following two-fold cross validation of 0.88 (Fig. 3).

Peritoneal tissue

Peritoneal tissue was collected from participants having primary surgery and participants having interval, post chemotherapy, surgery (IDS). The mean spectra of the pathology groups, benign and cancer and IDS benign (representing fibrosis) and IDS cancer are displayed in Fig. 4 and 5. As seen with ovarian tissue, separation within the groups is easily identifiable in this plot.

PCA-LDA model using the significant PCs on ANOVA testing (p = 0.001) achieved a sensitivity of 86% and specificity of 98% for classifying cancer from benign and cancer spectra of tissue taken at primary surgery. Leave one participant out cross validation of 441 benign and 245 cancer spectra achieved a sensitivity of 78% and specificity of 84%. The F1 score for this validation model was 0.83 and mean area under the curve following two-fold cross validation of 0.86 (Fig. 3).

In the group with spectra from tissue collected at interval debulking surgery, as seen in other cancer and benign comparisons, the difference between the mean spectra suggested increased intensity in phosphates (1103 cm^{-1} DNA stretch mode), DNA (827 cm^{-1}), amino acids (642, 1003, 1360 & 1597 cm^{-1}), lipids (1126 cm^{-1}), nucleic acids (665, 722, 779, 1332, 1485 & 1573 cm^{-1}), amide I (1658 cm^{-1} stretch mode) and a subtle uplift in carotenoids (1156 & 1526 cm^{-1}) in the cancer group, and lower concentrations of thymine (748 cm^{-1}), collagen (812, 867, 919 & 922 cm^{-1}), phenylalanine (1026 cm^{-1}), amide III beta sheet (1240 cm^{-1}), antisymmetric CH_3 deformation (1415 cm^{-1}), aromatic amino acids (1597 cm^{-1}) and amide I group (1628 & 1698 cm^{-1}) in the cancer group when compared to the benign group. The PCA-LDA model classified cancer from benign and cancer tissue (interval surgery) with a sensitivity of 81% and specificity of 91%. Leave one participant out cross validation of 931 benign and 931 cancer spectra achieved a sensitivity of 68% and specificity of 81%. The F1 score for this validation model was 0.73 and mean area under the curve following two-fold (50% training data and 50% held out) cross validation of 0.79 (Fig. 3).

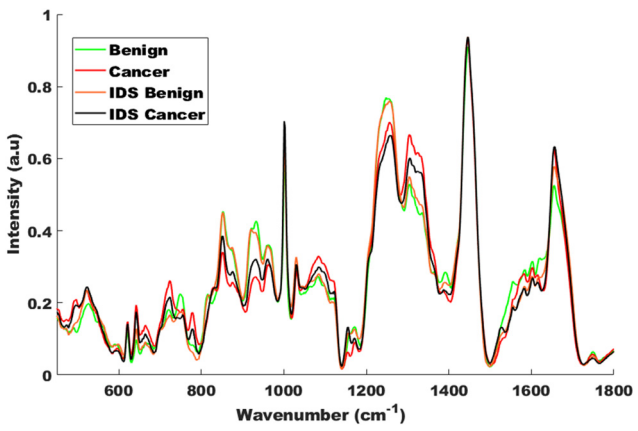

Fig. 4 Mean spectra of peritoneal tissue for the pathology groups benign (green), cancer (red) and, interval debulking surgery (IDS) groups, benign IDS (orange) and cancer IDS (grey).

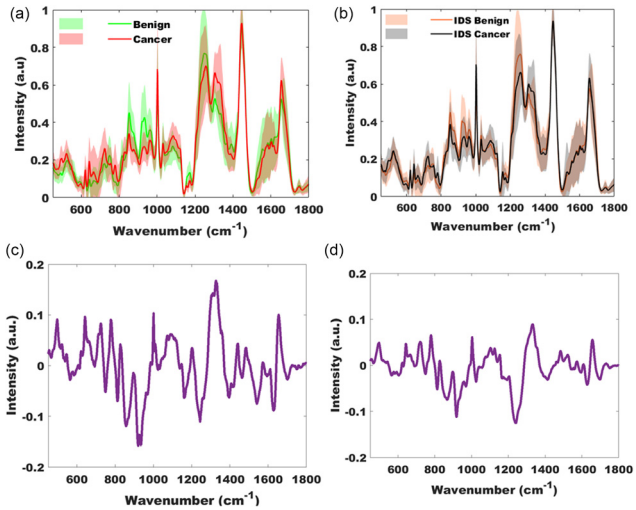

Fig. 5 Mean and standard deviation spectra of comparison of pathology groups for peritoneal tissue. (a) Cancer *versus* benign, primary surgery (686 spectra); (b) cancer *versus* benign, interval surgery (after chemotherapy) (1862 spectra); (c) and (d) are difference between spectra of the pathology groups from (a) and (b) respectively.

Discussion

Raman spectroscopy was used to determine the biomolecular composition of ovarian and peritoneal samples and correctly classified cancer from non-cancer with high accuracy. Difference between the mean spectra of the pathology groups broadly characterise the differences between cancer and non-cancer as increased nucleic acid activity, lipids and amino acids and decrease in collagen and carotenoids in cancer. The upregulation of lipids and amino acids has been reported in other work looking at metabolic changes in cancers, with dysregulation of lipids reported in hepatocellular carcinoma, bladder cancer and colorectal cancer.[23,24] Carotenoids have antioxidant properties and have been suggested to reduce tumour growth and induce apoptosis in cancer cells. Whilst conclusions cannot be drawn from limited work to date, there is consistent data showing low carotenoid levels in ovarian cancer.[25–27] The morphology and concentration of collagen I has been demonstrated to change in ovarian cancer with lower abundance of collagen seen in all epithelial cancer.[28]

The classification model in peritoneal tissue for the primary surgery group performed slightly better than the

primary chemotherapy group (AUC 0.86 *vs.* 0.79). Whilst the sample size was smaller in the primary surgery group, 17 *vs.* 38, it does not account for the difference in performance as a smaller sample size is more likely to cause a type II error as opposed to improving diagnostic performance. That said, both models achieved high cross validation accuracies for cancer detection suggesting that the potential impact of chemotherapy on diagnostic performance, if any, is small and Raman spectroscopy can accurately differentiate between fibrosis and cancer.

To our knowledge, this is the first work assessing borderline tumours with Raman spectroscopy. The extremely reassuring results for cancer classification (AUC 0.99) against borderline tissue makes a very promising case for translation of this technique to use in place of frozen section should tissue measurements with a portable device[29] yield similarly high accuracies. The availability of such a device could potentially decrease pathology workload and operative and anaesthetic time, with the biggest impact being in units that do not have pathology services in the same building or site as the operating theatre. As ovarian cancer surgery is currently an open surgical procedure, and the likely clinical application of a device would be intraoperative measurement excised areas of concerns, constraints of size of probe as seen in endoscopic devices does not apply however, these probes have demonstrated high accuracy in cancer detection and might offer a readily available first step to translation of this technique.[30–33]

In previous work looking at Raman spectroscopy of biological samples, two or three pathologists were consulted due to a known lack of consensus between pathologists for cancer and pre-cancer.[34] All participants had a formal histological diagnosis as part of their clinical care by one of the gynaecology pathologists at their respective hospital, and there was no discrepancy between their clinical diagnosis and the diagnosis given on assessment of their research samples by a second histopathologist. A potential limitation of this study is that only one pathologist was consulted for the identification of the specific location on the tissue at which Raman spectroscopy measurements were taken, however, this was considered a relatively trivial process.

Whilst overall recruitment for this study was on par with, if not higher than, previous work on ovarian cancer, a limitation of this work is the small participant numbers when comparing pathology groups. Consequently, meaningful independent group testing could not be performed.

Conclusion

Raman spectroscopy can accurately classify ovarian cancer from other tissue types and is non-destructive. It has strong potential as candidate for an intra-operative tool for residual disease volume assessment where a surgeon is unclear about areas of abnormality and as a replacement for frozen sections. *Ex vivo* measurements of tissue blocks using portable Raman devices could be the next step in optimising this technique for intra operative use. Whilst the technique can accurately classify post chemotherapy fibrosis from cancer, further work is required to understand why this slightly underperforms compared to peritoneal tissue from primary surgery.

Author contributions

Diana Frimpong – data curation, formal analysis, investigation, methodology, project administration, resources, software, validation, visualisation, writing original draft, writing review and editing. Angela C. Shore – supervision, writing (review and editing). Benjamin Gardner – software, writing (review and editing). Claire Newton – supervision, resources, writing (review and editing). Joya Pawade – supervision, resources, editing. Jonathan Frost – supervision, resources, editing. Laura Atherton – resources. Nick Stone – data curation, formal analysis, methodology, resources, software, supervision, validation, writing (review and editing).

Data availability

Data supporting this article have been included as part of the ESI.†

Conflicts of interest

There are no conflicts to declare.

Acknowledgements

Thanks go to all the staff in gynaecology clinics and operating department at St Michaels Hospital Bristol and Royal United Hospitals Bath, as well as Emmanuel Frimpong from Severn Pathology department.

References

1 NICE Guideline, Ovarian cancer: recognition and initial management (CG122): National Institute for Health and Care Excellence, 2011, Available from: **https://www.nice.org.uk/guidance/cg122/resources/ovarian-cancer-recognition-and-initial-management-pdf-35109446543557**.
2 Cancer Research UK, Ovarian Cancer Incidence, Available from: **https://www.cancerresearchuk.org/health-professional/cancer-statistics/statistics-by-cancer-type/ovarian-cancer#heading-Zero**.
3 Cancer Intelligence Team, Survival and Incidence by stage of diagnosis: Cancer Reseaech UK; Available from: **https://crukcancerintelligence.shinyapps.io/EarlyDiagnosis/**.
4 A. Elattar, A. Bryant, B. A. Winter-Roach, M. Hatem and R. Naik, Optimal primary surgical treatment for advanced

epithelial ovarian cancer, *Cochrane Database Syst. Rev.*, 2011, **2011**(8), Cd007565.
5 S. Kehoe, J. Hook, M. Nankivell, G. C. Jayson, H. Kitchener, T. Lopes, *et al.*, Primary chemotherapy versus primary surgery for newly diagnosed advanced ovarian cancer (CHORUS): an open-label, randomised, controlled, non-inferiority trial, *Lancet*, 2015, **386**(9990), 249–257.
6 I. Vergote, C. G. Tropé, F. Amant, G. B. Kristensen, T. Ehlen, N. Johnson, *et al.*, Neoadjuvant Chemotherapy or Primary Surgery in Stage IIIC or IV Ovarian Cancer, *N. Engl. J. Med.*, 2010, **363**(10), 943–953.
7 H. J. Butler, L. Ashton, B. Bird, G. Cinque, K. Curtis, J. Dorney, *et al.*, Using Raman spectroscopy to characterize biological materials, *Nat. Protoc.*, 2016, **11**(4), 664–687.
8 E. Smith and G. Dent, Introduction, Basic Theory and Principles, in *Modern Raman Spectroscopy – A Practical Approach*, 2004, pp. 1–21.
9 J. Haskell, T. Hubbard, C. Murray, B. Gardner, C. L. Ives, D. Ferguson, *et al.*, High wavenumber Raman spectroscopy for intraoperative assessment of breast tumour margins, *Analyst*, 2023, **148**(18), 4373–4385.
10 J. Horsnell, P. Stonelake, J. Christie-Brown, G. Shetty, J. Hutchings, C. Kendall, *et al.*, Raman spectroscopy–a new method for the intra-operative assessment of axillary lymph nodes, *Analyst*, 2010, **135**(12), 3042–3047.
11 A. Heintz, F. Odicino, P. Maisonneuve, M. Quinn, J. Benedet, W. Creasman, *et al.*, Carcinoma of the Ovary, *Int. J. Gynecol. Obstet.*, 2006, **95**(S1), S161–SS92.
12 J. S. Berek, M. Renz, S. Kehoe, L. Kumar and M. Friedlander, Cancer of the ovary, fallopian tube, and peritoneum: 2021 update, *Int. J. Gynecol. Obstet.*, 2021, **155**(S1), 61–85.
13 C. M. Krishna, G. D. Sockalingum, R. A. Bhat, L. Venteo, P. Kushtagi, M. Pluot, *et al.*, FTIR and Raman microspectroscopy of normal, benign, and malignant formalin-fixed ovarian tissues, *Anal. Bioanal. Chem.*, 2007, **387**(5), 1649–1656.
14 K. Maheedhar, R. A. Bhat, R. Malini, N. B. Prathima, K. Keerthi and P. Kushtagi, *et al.*, *Diagnosis of Ovarian Cancer by Raman Spectroscopy:A Pilot Study*, 2008.
15 S. David, A. Plante, F. Dallaire, J. P. Tremblay, G. Sheehy, E. Macdonald, *et al.*, Multispectral label-free Raman spectroscopy can detect ovarian and endometrial cancer with high accuracy, *J. Biophotonics*, 2022, **15**(2), e202100198.
16 C. Andreou, A. Oseledchyk, F. Nicolson, N. Berisha, S. Pal and M. F. Kircher, Surface-enhanced Resonance Raman Scattering Nanoprobe Ratiometry for Detecting Microscopic Ovarian Cancer via Folate Receptor Targeting, *J. Visualized Exp.*, 2019, **145**, e58389.
17 S. S. Buys, E. Partridge, A. Black, C. C. Johnson, L. Lamerato, C. Isaacs, *et al.*, Effect of Screening on Ovarian Cancer Mortality: The Prostate, Lung, Colorectal and Ovarian (PLCO) Cancer Screening Randomized Controlled Trial, *J. Am. Med. Assoc.*, 2011, **305**(22), 2295–2303.
18 K. Kumar, Principal component analysis: Most favourite tool in chemometrics, *Resonance*, 2017, **22**, 747–759.
19 L. Faes, X. Liu, S. K. Wagner, D. J. Fu, K. Balaskas, D. A. Sim, *et al.*, A Clinician's Guide to Artificial Intelligence: How to Critically Appraise Machine Learning Studies, *Transl. Vis. Sci. Technol.*, 2020, **9**(2), 7.
20 N. Stone, *Raman spectroscopy of biological tissue for application in optical diagnosis of malignancy*, Cranfield University, 2001.
21 C. A. Kendall, *A study of Raman spectroscopy for the early detection and classification of malignancy in oesophageal tissue*, Cranfield University, 2002.
22 A. C. S. Talari, Z. Movasaghi, S. Rehman and R. Iu, Raman Spectroscopy of Biological Tissues, *Appl. Spectrosc. Rev.*, 2015, **50**(1), 46–111.
23 D. W. Jeong, S. Lee and Y. S. Chun, How cancer cells remodel lipid metabolism: strategies targeting transcription factors, *Lipids Health Dis.*, 2021, **20**(1), 163.
24 Z. Li and H. Zhang, Reprogramming of glucose, fatty acid and amino acid metabolism for cancer progression, *Cell. Mol. Life Sci.*, 2016, **73**(2), 377–392.
25 J. L. Rowles and J. W. Erdman, Carotenoids and their role in cancer prevention, *Biochim. Biophys. Acta, Mol. Cell Biol. Lipids*, 2020, **1865**(11), 158613.
26 E. Czeczuga-Semeniuk and S. Wolczynski, Identification of carotenoids in ovarian tissue in women, *Oncol. Rep.*, 2005, **14**(5), 1385–1392.
27 V. Böhm, G. Lietz, B. Olmedilla-Alonso, D. Phelan, E. Reboul, D Bánati, *et al.*, From carotenoid intake to carotenoid blood and tissue concentrations - implications for dietary intake recommendations, *Nutr. Rev.*, 2021, **79**(5), 544–573.
28 M. Sarwar, P. H. Sykes, K. Chitcholtan and J. J. Evans, Collagen I dysregulation is pivotal for ovarian cancer progression, *Tissue Cell*, 2022, **74**, 101704.
29 O. Stevens, I. E. Iping Petterson, J. C. C. Day and N. Stone, Developing fibre optic Raman probes for applications in clinical spectroscopy, *Chem. Soc. Rev.*, 2016, **45**(7), 1919–1934.
30 J. C. Day, R. Bennett, B. Smith, C. Kendall, J. Hutchings, G. M. Meaden, *et al.*, A miniature confocal Raman probe for endoscopic use, *Phys. Med. Biol.*, 2009, **54**(23), 7077–7087.
31 L. M. Almond, J. Hutchings, G. Lloyd, H. Barr, N. Shepherd, J. Day, *et al.*, Endoscopic Raman spectroscopy enables objective diagnosis of dysplasia in Barrett's esophagus, *Gastrointest. Endosc.*, 2014, **79**(1), 37–45.
32 P. Crow, N. Stone, C. A. Kendall, J. S. Uff, J. A. M. Farmer, H. Barr, *et al.*, The use of Raman spectroscopy to identify and grade prostatic adenocarcinoma in vitro, *Br. J. Cancer*, 2003, **89**(1), 106–108.
33 A. Molckovsky, L. M. Song, M. G. Shim, N. E. Marcon and B. C. Wilson, Diagnostic potential of near-infrared Raman spectroscopy in the colon: differentiating adenomatous from hyperplastic polyps, *Gastrointest. Endosc.*, 2003, **57**(3), 396–402.
34 N. Stone, C. Kendall, J. Smith, P. Crow and H. Barr, Raman spectroscopy for identification of epithelial cancers, *Faraday Discuss.*, 2004, **126**(0), 141–157.